

# The mechanical response of semi-exible networks to localized perturbations

D A . Head<sup>1,2</sup>, A J. Levine<sup>3</sup> and F C . M acK intosh<sup>1</sup>

<sup>1</sup> D epartment of Physics and A stronomy, V rije U niversiteit, A msterdam , The N etherlands.

<sup>2</sup> D epartment of Applied Physics, T he U niversity of Tokyo, Tokyo 113-8656, Japan.

<sup>3</sup> D epartment of Physics, U niversity of M assachusetts, Amherst M A 01060, U SA .

D ated: February 8, 2020

P revious research has suggested that semi-exible gels, e.g. cross-linked F -actin, admit a new mesoscopic length scale associated with the length scale below which one observes significant deviations from the affine deformation of the network under uniformly applied external strain. In this paper we extend this study of the mechanics of semi-exible gels by examining the Young's modulus of such materials and by studying the response of these networks to localized forces and force dipoles. We show that the nonaffinity length [D A . Head et al. P RE 68, 061907 (2003).] controls the mesoscopic response to point forces and the crossover to continuum elastic behavior at large distances. In the immediate vicinity of the point force, other length scales regulating the network structure become relevant.

PACS numbers: 87.16.Ka, 82.35.Pq, 62.20.Dc

## I. INTRODUCTION

Semi-exible polymers such as lamellous proteins resemble elastic rods on a molecular scale, while exhibiting significant thermal fluctuations on the scale of micrometers or even less. This has made them useful as model systems allowing for direct visualization via optical microscopy. But, semi-exible polymers are not just large versions of their more well-studied exible cousins such as polystyrene. Filamentous proteins, in particular, have been shown to exhibit qualitatively different behavior in their networks and solutions. A fundamental reason for this is the fact that the thermal persistence length, a measure of lamellous stiffness as the length at which thermal bending fluctuations become apparent, can become large compared with other important length scales such as the spacing between polymers in solutions, or the distance between chemical crosslinks in a network.

One of the most studied semi-exible polymers in recent years has been F -actin, a lamellous protein that plays a key structural role in cells [1, 2]. These occur in combination with a wide range of specific proteins for crosslinking, bundling and force generation in cells. These composites, together with other lamellous proteins such as microtubules, constitute the so-called cytoskeleton that gives cells both mechanical integrity and structure. This biopolymer gel is but one example of a large class of polymeric materials that can store elastic stress in a combination of bending and extensional deformations of the constituent elements. We term these materials semi-exible gels or networks.

One of the important lessons from recent experimental and theoretical studies is that the shear modulus of cross-linked semi-exible networks bears a much more complex relationship to the mechanical properties of the constituent lamellous and to the microstructure of the gel than is the case for exible polymer gels [3]. Recently, it has been shown that semi-exible gels exhibit a striking cross-over [4, 5, 6, 7, 8] between a response to external

shear stress that is characterized by a spatially heterogeneous strain (a non-affine regime [9]) and a uniform strain response (an affine regime [10]). This crossover is governed primarily by cross-link density or molecular weight (lamellous length). The effective long length scale shear modulus of the network simultaneously increases by about six orders of magnitude at this nonaffinity-to-affine cross-over. The underlying mechanism responsible for this abrupt cross-over appears to be the introduction of a new, mesoscopic length scale in the problem that is related to both the thermal persistence length of the constituent polymers and the mean spacing between consecutive cross-links along the chain [4, 7].

One can associate this mesoscopic length with the length below which the deformation of the network departs from the standard affinity [7]. The macroscopic shear response of the network is controlled by a competition between this new length scale (the nonaffinity length) and the lamellous length,  $L$ . On the one hand, when the lamellous length is long, nonaffine corrections to the deformation field, which are localized to regions within of the lamellous ends, do not control the mechanical properties of the network; the shear modulus of the macroscopic system is well-described by calculations based on a linear deformation reflecting the fact that nonaffine deformations of the lamellous ends are subdominant corrections in this limit. Moreover, the elastic energy is stored primarily in the (homogeneous) extension and compression of lamellous. On the other hand, when the lamellous are of a length comparable to, or shorter than the nonaffinity length, i.e.  $L <$  then the nonaffine deformations of the ends play a large role in the determination of the mechanical properties of the network. The network is found to be generally more compliant, and the elastic energy under applied shear stress is stored in a spatially heterogeneous manner in the bending of lamellous. The existence of these distinct regimes as a function of lamellous length reflects a fundamental difference of these semi-exible polymer networks with respect to

their flexible counterparts: polymers can maintain their mechanical integrity and state of stress/strain across network nodes or crosslinks.

These results naturally lead one to pose a number of basic questions regarding the elastic properties of semi-flexible networks. While these random networks must on basic theoretical grounds appear as continuum, isotropic materials at the longest length scales, these considerations do not predict the length at which the continuum approximation applies. The previous identification of the nonlinearity length, as a mesoscopic length uniquely associated with semi-flexible networks suggests that this length controls the cross-over to continuum behavior [7]. After all the annealing of the network under uniform stress at scales large compared to shows that in one case at least the nonlinearity length controls the cross-over to continuum behavior. One of the principal results of this work is the demonstration that more generally controls this cross-over to continuum mechanics in semi-flexible gel systems.

Prior work has focussed exclusively on simple shear and uniaxial extension. In order to better examine the universality of the previous results, we study the opposite limit of a highly localized external force in the form of a point force monopole or dipole. If one can show that the elastic (displacement) Green's function of the system similarly depends on only one additional parameter then it would appear that this quantity completes the coarse-grained elastic description of the system on all length scales down to the mean distance between crosslinks. It may be, however, that the deformation field of these semi-flexible networks is much more complex and the simplification introduced by in the description of the network's response to uniform shear strain cannot be generalized to deformations resulting from more general forcing conditions.

While our results below, indeed, show that does largely control the crossover to (the far field) continuum elasticity, in the observed elastic Green's function is sensitive to the local structure of the network on length scales below . Below we discuss how we quantify the structure of the Green's function and its approach to the form required by continuum elasticity. The observed elastic Green's function, however, depends not only on the dependent Langevin clients of the material, but also on local properties of the displacement field in immediately surrounding the the point force. In effect one may imagine that, upon the application of the point force, the network acts as a type of composite material: within a distance of the point force it deforms in a way not well described by continuum theories, while outside of that zone it does appear to act like an elastic continuum. The Green's function depends of course on the material properties of both media. Unfortunately only one of those media (the outer zone) is well characterized by the simple continuum theory of an isotropic elastic solid, so the complete Green's function remains complex and depends on the detailed network structure within the inner zone

surrounding the applied force.

There is another set of questions that may be addressed via the study of the network's response to point forces and force dipoles. Such forces not only probe the material properties of the network in a manner complementary to the uniform strains explored earlier, they also have direct physical implications for microrheology in F-actin networks and for the dynamics of the cytoskeleton in response to the activity of nanoscale molecular motors, e.g. myosin. Fluctuation-based microrheology, an application of the fluctuation-dissipation theorem to the study of rheology via the statistical analysis of the thermally fluctuating position of sub-micron tracer particles embedded in the medium, requires one to understand the elastic Green's function of the medium. Thus understanding the response of semi-flexible networks to localized forces has direct experimental implications and consequences for force production in the cytoskeleton.

In this biological context, the semi-flexible network making up the cytoskeleton is generally found in association with molecular motors that, to a good approximation, generate transient localized force dipoles in the material. To both understand force generation in the cell as well as the material properties of these cytoskeletal networks driven into nonequilibrium steady states by these molecular motors, one must determine the displacement field associated with such motor-induced forces.

Notwithstanding our biological motivation for this work, our findings also bear on the broader problem of elastic modes in amorphous materials. It has been shown that the vibrational modes of deep (quenched Lennard-Jones systems) approach a continuum description only on scales exceeding some mesoscopic length [11, 12]; for the protocols considered, a value 30 particle dimensions was robustly found. This was physically identified with a length scale for nonlinearity, suggesting a direct correspondence with our (although our can be controlled by varying the mechanical properties of the constituents). A comparable length was also found to control the self-averaging of the Green's function to the form expected by continuum elasticity [13]. These findings for radially interacting particles are broadly in keeping with our own investigations for semi-flexible polymer networks.

The remainder of this paper is organized as follows: In section II we develop our model of semi-flexible, permanently cross-linked gels, summarize the numerical simulations used to study it, and discuss the expected structure of the displacement field when averaged over numerous realizations of the network. In section III we report our results for both point forces in IIIA and force dipoles in IIIB. We then discuss our studies of the bulk elastic properties of these networks in IIIC before concluding in section IV.

## II. MODEL

### A. The semi-exible network

A highly successful continuum continuum model of individual semi-exible polymers is the worm-like chain. This treats the linear lam ents as elastic rods of fixed contour length and negligible thickness, so that the dominant contribution to the elastic energy comes from bending modes and the Ham iltonian linearized to small deviations from a straight con guration that is given by

$$H^2 = \frac{1}{2} \int^Z (r^2 u)^2 ds; \quad (1)$$

where  $u$  is the transverse displacement of the lam ent relative to an arbitrary straight axis,  $s$  is its arc length, and the elastic modulus gives the bending energy per unit length  $s$ .

The longitudinal response of the worm-like chain model is calculated from the increase in free energy due to an extensional stress applied along the mean lam ent axis [10, 14]. However, the numerical algorithm used in our simulations is based on the minimization of the Ham iltonian of the system, and hence is fundamentally athermal. The reason for this choice is essentially one of efficiency: assuming there are no subtle convergence issues, minimization is expected to be faster than stochastic modelling and, it is anticipated, give better statistics for a given C P U time. This does, however, mean that the entropic mechanism governing the longitudinal response is absent, and an explicit energetic term is required.

An unconstrained lam ent at  $T = 0$  forms a straight con guration, and thus elongation of its end-to-end distance must be accompanied by a change in the absolute contour length. It is therefore natural to incorporate longitudinal modes by adding a second elastic term to the Ham iltonian for the extension or shortening of the lam ent backbone,

$$H^k = \frac{1}{2} \int^Z \frac{dl(s)}{ds}^2 ds; \quad (2)$$

where  $dl(s)/ds$  gives the strain or relative change in local contour length, and  $k$  is the Young's modulus of the lam ent (essentially a spring constant normalized to  $1/[\text{length}]$ ). Of course, such modes also exist in thermal systems, but may be dominated by the entropic spring term [10], except possibly for very short lam ent segments or very densely cross-linked gels. The connection between thermal/entropic and athermal longitudinal compliance is discussed in greater detail in Ref. [7].

The two elastic coe cients and together define a length scale  $l_b = \sqrt{k} = \sqrt{2}$ , which we will shall refer to as the intrinsic bending length by observing that an isolated lam ent constrained to have different tangents at its end points will deform with this characteristic length. To avoid potential confusion, however, we note that this is not the typical length scale for bending deformations of

a semi-exible lam ent. Rather, the bending energy of lam ents tends to make the longest unconstrained wavelength bending mode the dominant one. Thus, for instance, in a crosslinked gel, lam ents are expected to be bent primarily on a length comparable to the distance between crosslinks. Nonetheless  $l_b$  is a useful measure of lam ent rigidity, in that large  $l_b$  corresponds to rigid lam ents, and small  $l_b$  to exible ones.

Although and have been introduced as fundamental parameters, if the lam ent is regarded as a continuous elastic body with uniform cross section at zero temperature, then they can both be expressed in terms of the characteristic lam ent radius  $a$  and intrinsic bulk modulus  $Y_f$  as  $Y_f a^4$  and  $Y_f a^2$ . Thus  $l_b = a$ , and thinner lam ents are more exible than thick ones (as measured by  $l_b$ ), as intuitively expected. Given the possibility of entropic effects in , however, we shall treat these as independent parameters of the theory [7].

The gel is constructed by depositing lam ents of monodisperse length  $L$  and zero thickness onto a two-dimensional substrate. The center of mass position vector and orientation of the lam ents are uniformly distributed over the maximum allowed range, so the system is macroscopically isotropic and homogeneous. Whenever two lam ents overlap they are cross-linked at that point. Deposition continues until the required mass density, as measured by the mean distance between crosslinks  $l_c$ , has been reached. The network thus constructed can be described by three lengths:  $L$ ;  $l_b$ , and  $l_c$  and one modulus scale:  $k$ . In two-dimensions  $l_c$  characterizes both the mass density and cross-link density in spatially random, isotropic networks. The length  $l_b$  characterizes the mechanical properties of the constituent lam ents via the ratio of their bending to stretching compliance. The overall modulus scale will be absorbed into the point forces applied to the network.

In order to apply the point forces, a crosslink is chosen at random and identified as the origin of the system; it is this crosslink that will later be perturbed. A fixed circular boundary at radius  $R$  from the origin is imposed, and any lam ents or lam ent segments that extend beyond the boundary are simply removed or truncated, respectively.

### B. Numerical method

Details of the simulation method have been presented elsewhere [7]. Here we briefly summarize the procedure, with particular attention on those aspects that are central to the problems studied in this paper.

The system Ham iltonian  $H(f_x, g)$  is constructed from discrete versions of (1) and (2) applied to the geometry generated by the random deposition procedure described above. The degrees of freedom  $f_x, g$ , or nodes, are the position vectors of both crosslinks and midpoints between crosslinks, the latter so as to incorporate the first bending mode along the lam ent segments. Additional nodes

could be included at the cost of additional run time, but are expected to have a small effect, since the longest unconstrained wavelengths tend to dominate bending deformations. Crosslinks are treated as constraints on the relative position of each connected lamellar segment, but not on their relative rotation. Physically this corresponds to an inextensible but freely rotating linkage. As previously noted, constrained bending at crosslinks has a small effect except at high network concentrations (specifically, when  $l_c$  becomes comparable to  $a$ ) [7]. Nodes on the boundary are immobile. Note that, as in our earlier work [4, 6, 7], the network is assumed to be initially unstressed on both macroscopic and microscopic length scales.

There are two ways in which the system may be perturbed. The first, which we call monopole forcing, is to apply an arbitrarily small external force  $\mathbf{f}^{ext}$  to the crosslink at the origin. The network is then allowed to relax to a new configuration consistent with mechanical force balance at every node. The second, which we call dipole forcing, is to introduce a geometrical defect into the system by moving the central crosslink along the contour length of one of the lamellae to which it belongs, but not the other. Physically, this corresponds, e.g., to a motor introducing relative motion of one lamellae with respect to another lamellae. In the simulations, this effect is incorporated by infinitesimally 'shifting' the image of the central node with respect to other nodes on one lamellae.

Once the perturbation has been specified, the displacements of the nodes in the new mechanical equilibrium are calculated by minimizing the system Hamiltonian  $H(\mathbf{f}, \mathbf{g})$  using the conjugate gradient method [15]. This generates a displacement field for the particular geometry under consideration, as shown in Fig. 1. Note that  $H(\mathbf{f}, \mathbf{g})$  is linearized about small nodal displacements  $\mathbf{f}_i$  from their original positions  $\mathbf{f}_i$ , so linear response is assured. The bulk response to non-linear strains has been recently studied by Ondek et al. [16].

### C. Decomposition of mean displacement field

As shown in Fig. 1, the displacement field for a particular network is quite complex and generically shows anti-correlations between displacements and the local mass distribution. Although these fluctuations reflect inherent and possibly interesting physical properties of the gels, a more basic and immediately applicable quantity to measure is the mean displacement field, found by averaging many individual runs with differing geometries but identical system parameters  $R$ ,  $L$ ,  $l_c$  and (or equivalently  $R$ ,  $L$ ,  $l_c$  and  $l_b$ ). Two examples for differing (the radius of the green circle centered on the point of force application) are given in Fig. 2. These plots demonstrate one of the primary results of this paper, namely that the crossover between continuum (or quasi-continuum) response at large lengths, to a more exotic displacement

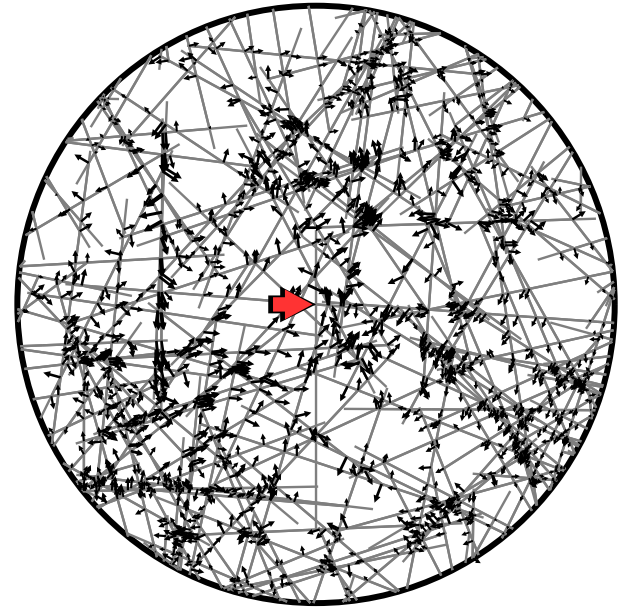


FIG. 1: (Color online) An example of a network of lamellae of uniform length  $L$  (grey line segments) perturbed by an external force, denoted by the large red arrow, applied to the crosslink at the origin of a circular system of radius  $R = L$ . The arrow lengths are logarithmically calibrated to the magnitude of the displacement of each crosslink. In this example,  $L = l_c = 29.1$ ,  $a = L = 0.191$  and the force is perpendicular to one of the lamellae that form the central crosslink; forces can also be applied parallel to a lamellae.

field at shorter lengths, happens at a length of order  $(a)$  with a prefactor close to unity.

In order to precisely describe the structure of the deformation field, we consider its most general possible form. For monopole forcing, the displacement field  $\mathbf{u}(\mathbf{r})$  at position vector  $\mathbf{r}$  relative to the origin can be projected onto 3 other vectors, namely the direction of the external force  $\hat{\mathbf{f}}$ , the unit position vector  $\hat{\mathbf{r}}$  and the axis  $\hat{\mathbf{n}}$  of one of the lamellae to which the crosslink is attached,

$$\mathbf{u}_i = G_{ij} \hat{\mathbf{f}}_j; \quad G_{ij} = \frac{f}{a} \sum_{\alpha} g^{(\alpha)} \hat{\mathbf{r}}_i \hat{\mathbf{r}}_j + g^{(n)} \hat{\mathbf{n}}_i \hat{\mathbf{n}}_j + g^{(f)} \hat{\mathbf{f}}_i \hat{\mathbf{f}}_j \quad (3)$$

where  $f$  is the magnitude of the external force, and  $a$  is the shear modulus as predicted for a fine deformation. This depends on  $L$  and  $l_c$  but not  $l_b$ , and is included here to factor out the density dependence of the response. As defined, the  $g^{(\alpha)}$  (and the  $h^{(\alpha)}$  below) are dimensionless quantities in two dimensions.

Each  $g^{(\alpha)}$  can be further decomposed into angular modes in  $\theta$ , where  $\cos \theta = \hat{\mathbf{n}} \cdot \hat{\mathbf{f}}$ ,

$$g^{(\alpha)} = g_0^{(\alpha)} + 2 \sum_{m=1}^{\infty} g_m^{(\alpha)} \cos(m\theta); \quad m > 0; \quad m \text{ even} \quad (4)$$

Terms in  $\sin(m\theta)$  vanish since the ensemble-averaged response must be invariant under  $\theta \rightarrow -\theta$ , and  $\cos(m\theta)$

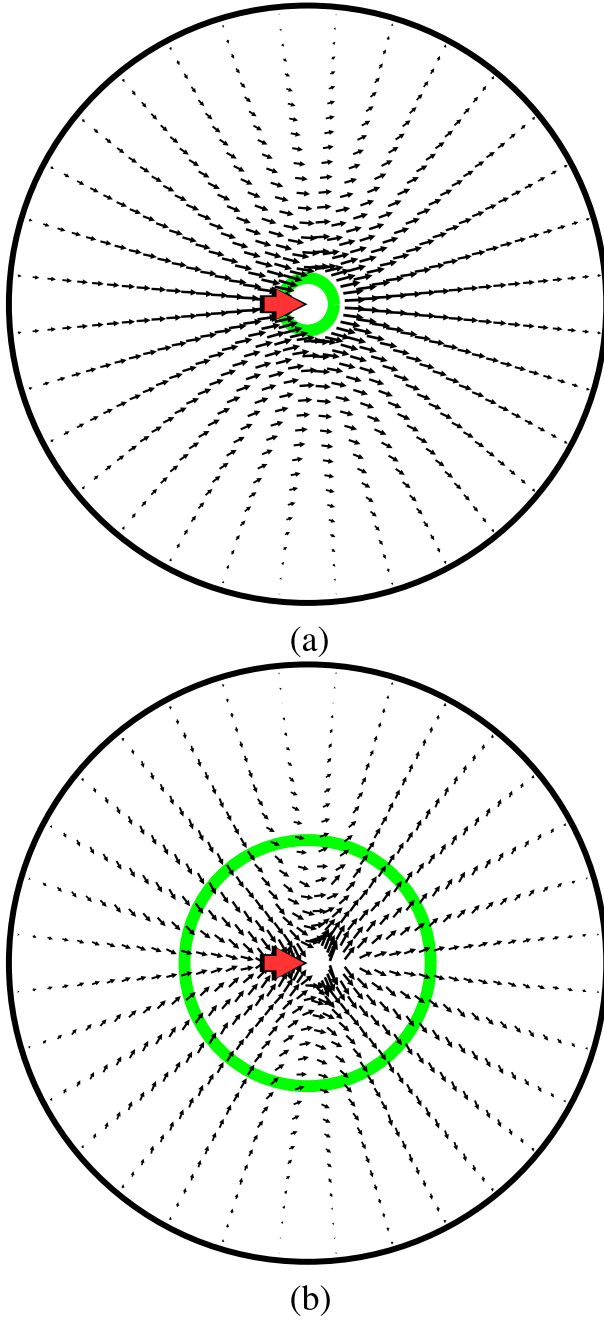


FIG. 2: (Color online) Mean response after averaging  $10^5$  networks with the same parameters as in Fig. (1) (including one lamella fixed perpendicular to the external force) except for  $\lambda$ , which is (a)  $\lambda = L = 0.089$  and (b)  $\lambda = L = 0.42$ . For easy visualization, a green circle of radius  $\lambda$  has been inserted into the background of each plot. Vectors near the center of each system have not been plotted for clarity.

terms with  $m$  odd also vanish due to  $\hat{n} \cdot \hat{n}$  invariance. This latter symmetry may appear to violate the known polarity of typical semi-flexible biopolymers such as F-actin and microtubules [17]; however, we are interested here in the mechanical properties of the lamellae, which, within the approximations of our model, are in-

deed invariant under  $\hat{n} \rightarrow -\hat{n}$ .

For dipole forcing, the above procedure is followed with the additional simplification that  $\hat{n}$  is proportional to  $\hat{f}$ , since the displacement (and hence force) dipole induced by the motion of a motor will always be parallel to one lamella axis. The decomposition is therefore somewhat simpler,

$$u_i = H_{ij}\hat{n}_j; \quad H_{ij} = \frac{f}{a} \sum_{m=0}^n h^{(r)}_{ij}\hat{e}_i\hat{e}_j + h^{(n)}_{ij}; \quad (5)$$

The scalar  $f$  is the magnitude of the force dipole; since it is actually a displacement that is imposed,  $f$  is unknown and will be treated as a fitting parameter. The angular decomposition is identical to before,

$$h^{(r)} = h_0^{(r)} + 2 \sum_{m=2, \text{ even}}^X h_m^{(r)} \cos(m\theta); \quad (6)$$

Later sections will refer to the continuum solution for each of the two forms of forcing. These are given in the appendix. For the monopole case, only two continuum modes are non-zero, namely  $g_0^{(r)}$  and  $g_0^{(f)}$ . The dipole modes are slightly more subtle: after averaging of many dipole fields generated by the simulation, the resulting field is quadrupole. This is an immediate consequence of the means of forcing the system. Recall that in an elementary step, a motor moves parallel to one lamella axis. This has the effect of compressing the lamella in front of the dipole, while stretching the trailing segment. Thus two lamella segments are perturbed, each of which can be treated as a force dipole which, for a particular network geometry, will be of different magnitudes and hence the resulting field is dipole. However, the net bias of this dipole is symmetrically distributed around zero, and thus vanishes after averaging, leaving a quadrupole field as shown in Fig. 3. As derived in the appendix, the non-zero modes for this field are  $h_0^{(r)}$ ,  $h_2^{(r)}$ ,  $h_0^{(f)}$  and  $h_2^{(f)}$ .

### III. RESULTS

The mechanical response to a localized perturbation depends on the distance from the point of perturbation. We divide the discussion of these results into the behavior of the network in the "near-field" regime (the immediate vicinity of the applied force) and the "far-field" regime (far from the point force). Finally we examine the bulk or macroscopic elastic properties of the network under uniformly imposed deformation. At large length scales, a continuum or quasi-continuum form is found in which only a small number of ensemble-averaged modes are non-vanishing. We find that  $\lambda$  again plays a central role in controlling the cross-over from the near-field to the intermediate region and in determining the macroscopic modulus of the network.

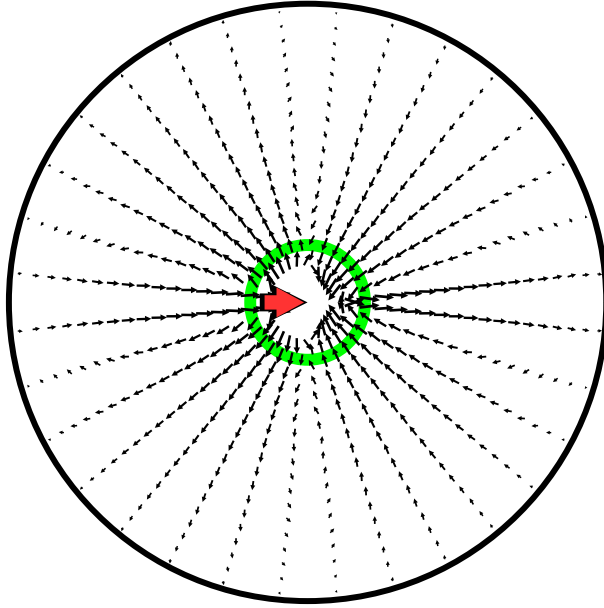


FIG. 3: (Color online) Mean displacement field after averaging over  $0(10^5)$  individual fields induced by imposing a displacement dipole at the origin. The orientation of the dipole is given by the red arrow. As explained in the text, the mean dipole moment vanishes after averaging and the resulting field is quadrupole. A green circle at a radius  $= 0.191L$  from the origin is also shown.

### A. The response to point forces

#### 1. Local behavior

In this section we focus on the short length scale behavior of the monopole response, for which the continuum form breaks down in two ways: (i) higher angular modes  $g_m^{(r)}$  and  $g_m^{(f)}$  with  $m > 0$  are non-zero, and (ii) the  $g_m^{(n)}$  modes do not vanish, i.e. the response depends on the orientation of the lamella to which the force is applied. This latter observation gives a clear example of how the response can 'see' the microscopic structure of the gel on short length scales.

An example demonstrating the appearance of higher modes at short lengths is given in Fig. 4, which shows the  $g_2^{(f)}$  mode for systems with different crosslink densities  $L=L_c$  but with the lamella flexibility chosen to give the same  $=L=0.191L$  in each case. Similarly, Fig. 5 shows the same mode for  $=L=0.089$ . In both cases,  $g_2^{(f)}$  becomes close to zero beyond a length comparable to  $L$ . No data is shown for larger values of  $L=L_c$  since at high network densities the numerical convergence of the strain field is so slow as to prevent attaining meaningful statistics with current processor power. For all network densities studied it is clear that the magnitude of  $g_2^{(f)}$  vanishes rapidly with distance from the point force.

Of course the disappearance of this term is required by continuum elasticity theory. From a comparison of

Fig. 4 and Fig. 5 it appears that the decay rate of this term is controlled by the nonlocal length,  $L$ . In order to demonstrate this more clearly, we plot  $g_2^{(f)}$  vs.  $r=L$  on a log-linear scale for various values of  $L$  in Fig. 6. The solid line corresponds to  $e^{-r/L}$ . The crossover from the more complex near-field regime is clearly governed by  $L$ .

This picture of higher modes decaying to near zero at a length comparable to  $L$  holds also for the  $m > 2$  modes of  $g_m^{(f)}$  and for all the  $m > 0$  modes of  $g_m^{(r)}$ . For reasons of space we do not show these data here. However, one example of a non-zero  $g^{(n)}$  mode will be given here, as this represents a qualitatively different sort of deviation from the expected continuum or far-field form. The  $g_0^{(n)}$  mode for  $=L=0.191$  is plotted in Fig. 7, and demonstrates similar behavior to the  $m > 0$  far-field modes discussed above.

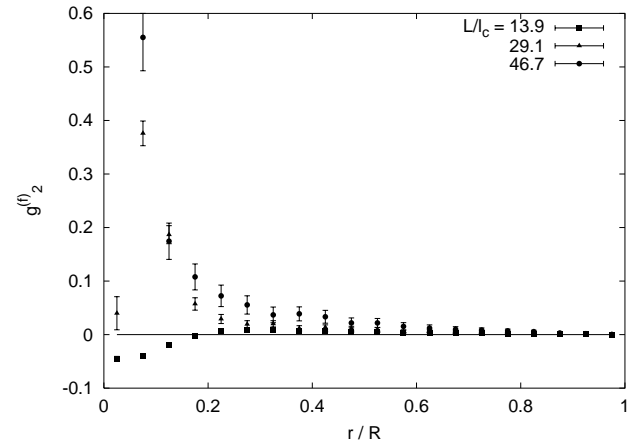


FIG. 4:  $g_2^{(f)}$  (which is dimensionless) versus distance from point of force application  $r$  for systems with the same  $=L=0.191$  and crosslink densities  $L=L_c$  as given in the key ( $L$  is the lamella length). The system radius  $R=L$  in all cases.

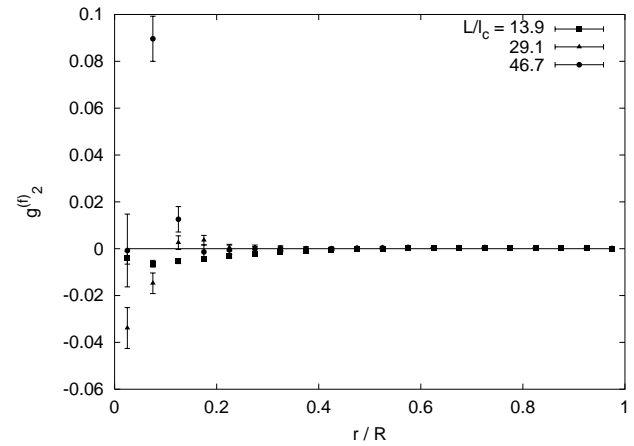


FIG. 5:  $g_2^{(f)}$  versus  $r=R$  for  $=L=0.089$  and differing  $L=L_c$ . The system radius  $R=L$ .

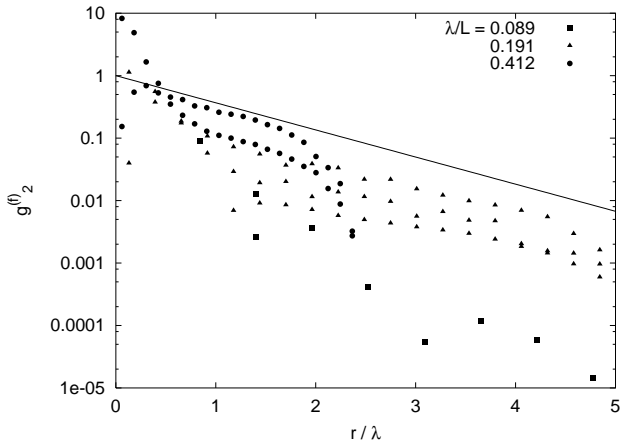


FIG. 6: Log linear plots of  $g_2^{(f)}$  versus the scaled distance from perturbation  $r =$  for system with various values of  $\lambda$  as given in the key. The system radius  $R = L$  in all cases.

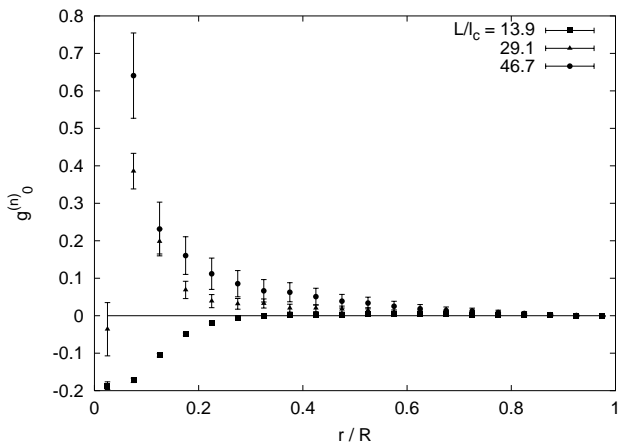


FIG. 7:  $g_0^{(n)}$  versus  $r=R$  for  $L=0.191$ ,  $R = L$  and the  $L/l_c$  given in the key.

Another instructive measure of the monopole response is the density of elastic energy  $E$  at a given distance from the point perturbation, which measures gradients of the displacement field and therefore complements the analysis of  $u(x)$  given above. In addition, since the simulation contains explicit terms for the transverse and longitudinal lamellar deformation modes, it is straightforward to plot the partitioning of the energy between these modes. Based on previous work [4, 5, 7], under homogeneous shear strain the partitioning of elastic energy between the bending and stretching modes of the lamellae is determined entirely by the  $\lambda$  to  $\lambda$  crossover. The ratio of  $L = \lambda$  was found to control this energy partitioning at a macroscopic or average level. It remains to be seen how this partitioning of the elastic energy occurs in vicinity of a point force.

The freedom to choose the angle between the point force and the direction of the lamellar to which that force is applied allows one to determine locally the partition-

ing of the elastic energy between bending and stretching modes of the lamellae. Forces directed along the lamellar axis generate primarily stretching deformations in the immediate vicinity of the origin (where the force is applied). Forces directed perpendicular to the lamellar axis, however, locally create a large bending deformation. As seen in the previous homogeneously imposed strain deformation calculations, for any given value of  $L = \lambda$  the network responds very differently to the bending or stretching deformations. Thus it is not surprising that the decay of the energy density from the point of force application to the boundary is strongly dependent on whether the force is applied parallel or perpendicular to one of the lamellae at the crosslink.

Fig. 8 shows  $E$  for parallel forces, where  $\lambda$  is fixed but the lamellar density  $L = l_c$  varies. There is an approximate data collapse onto a single curve as shown. The most notable discrepancy occurs near the boundary, where the low density data remains higher than those for larger  $L = l_c$  values. This is most likely an artefact of the fixed displacement boundary conditions, a point we shall return to later.

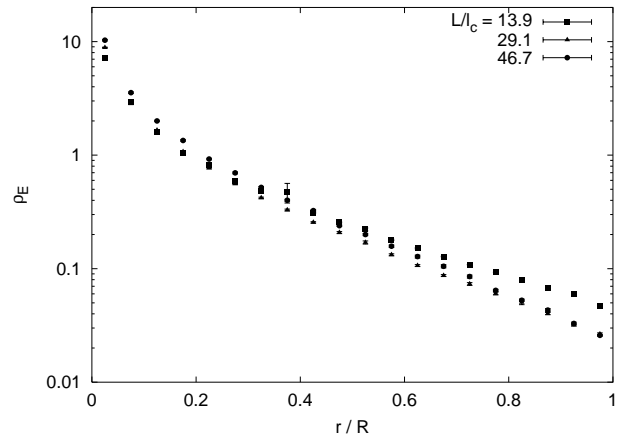


FIG. 8: Density of elastic energy  $E$  (in arbitrary units) versus distance  $r$  from an externally applied force that is directed along the lamellar to which it is applied.  $L = l_c$  is varied as given in the key, but  $R = L$  and  $\lambda = L = 0.191$  in all cases.

In contrast,  $E$  for forces perpendicular to a lamellar exhibits much richer behavior, as shown in Fig. 9, which shows the same data plotted against  $r = l_c$  and  $r = \lambda$ . For large distances, the data for different  $L = l_c$  appear to differ by only a scale factor. Since there is one arbitrary multiplicative factor for each curve (as only the magnitude of the applied force is fixed, not its displacement and hence work done on the network), these portions of the curves can be made to collapse after scaling, as in the parallel force case, suggesting that beyond some near-field regime, the decay of elastic energy density is once again exponential and governed by  $\lambda$  (see Fig. 9 lower panel). However, in this near-field regime for perpendicular forces there is clearly no possibility of such a collapse. Instead, it appears that the more rapid decay of elastic

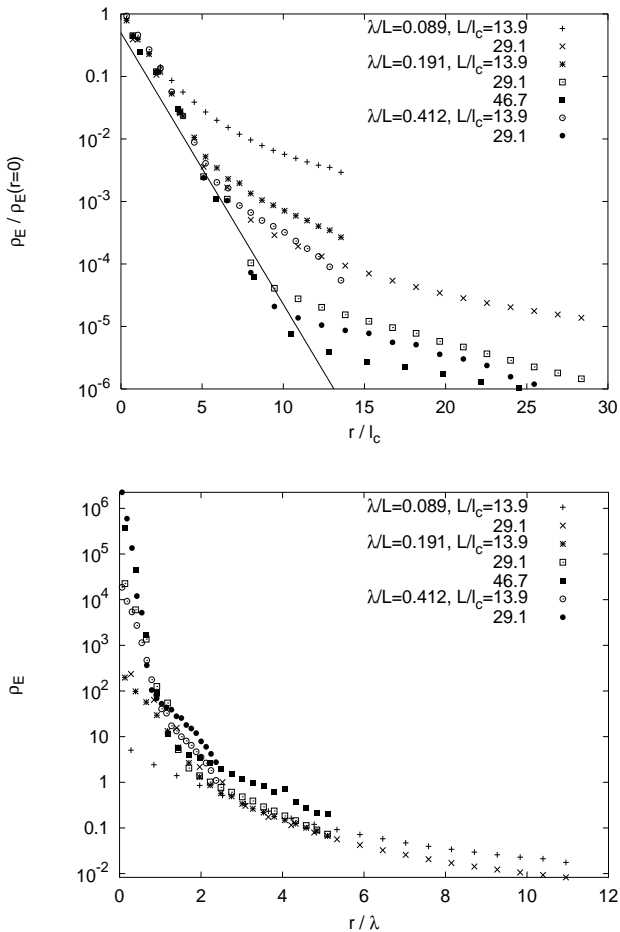


FIG. 9: Scaled elastic energy density versus distance from the point force for a variety of networks (see legend). In each case the force is directed perpendicularly to the lamellae where it is applied. In the upper panel distances are scaled by  $l_c$  and the data has been collapsed in the small  $r=l_c$  regime. The solid line is proportional to  $\exp(-r/l_c)$ , showing  $l_c$  controls the initial decay of elastic energy. In the lower panel the same energy densities are plotted against distance scaled by  $\lambda$ . This shows the energy density decays with that characteristic length scale at longer ranges. Error bars are not shown for reasons of clarity.

energy density in this near-eld regime is governed by the length  $l_c$ , as can be seen in the upper panel of Fig. 9 where the (rescaled) energy density data are plotted vs.  $r=l_c$  and shown to decay as  $\exp(-r/l_c)$  for distances  $r < 5l_c$  (ignoring finite size effects).

Based on the two different regimes of data collapse shown in Fig. 9, we conclude that there is a near-eld regime in which the decay of elastic energy is governed by a microscopic length scale (the mean distance between cross-links) and a longer-range regime in which the spatial decay of elastic energy density is controlled by the mesoscopic length  $\lambda$ . To better study this cross-over, we examine the partitioning of elastic energy between bending and stretching modes of the lamellae. Recall that in

the a ne limit, the elastic energy is stored primarily in the stretching and compression of the lamellae. In the nonaffine regime, on the other hand, the elastic energy is stored almost entirely in bending modes of the lamellae.

Plotted in Fig. 10 is the proportion of elastic energy due to longitudinal lamellar deformation for the perpendicular force case. Three data sets are displayed having different values of  $l_c$  and  $\lambda$  (see figure caption). The distance from the point of force application has been scaled by the geometric mean of  $l_c$  and  $\lambda$  leading to the observed coincidence of the crossover between regimes in the data. Close to the point of the application of the force, the displacement response is clearly dominated by bending modes of the lamellae. This is to be expected since the perpendicularly directed force directly injects bending energy into the system at the origin (the point of force application). The energy partitioning is inconsistent with that which is expected based on previous homogeneous shear measurements. From that work, one expects the network to determine the energy partitioning based only on the ratio:  $L = l_c$ . We observe the fraction of stretching energy to rapidly increase towards the expected value based on  $L = l_c$  [4, 7] and we may characterize each curve as having a 'knee' separating the region of varying energy ratio from a nearly constant intermediate regime where the partitioning of elastic energies corresponds well with the previously identified fraction of stretch/compression energy under macroscopic strain. This correspondence is demonstrated in Fig. 11. The horizontal lines show the fraction of stretching energy in periodic systems subjected to macroscopic shear, and clearly coincide with the plateau reached beyond the knee. At the largest distances one notices the vanishing of bending energy as the fraction of stretching energy approaches unity. This last effect is due to the fact that each lamella has a freely rotating bond at the outer, rigid wall. As this wall cannot support torques, the bending energy vanishes in a boundary layer whose width is determined by the mean distance between cross-links. We return to this point below.

The observed coincidence of the knees of all three curves under the rescaling of distances by  $\sqrt{l_c \lambda}$  suggests that this length sets the scale over which injected bending energy is redistributed into the combination of bending and stretching appropriate for long-length scale deformations.

Based on these observations we note that in all networks the strain field acquires the structure of the point force response based on continuum elasticity over a (typically mesoscopic) length scale of  $\lambda$ . When the networks is subjected to large, local bending deformations, however, it readjusts the partitioning of bending to stretching energy over a generally much shorter length scale,  $l_c$ . Thus the system is able to repartition the local elastic energy storage to the value appropriate for its  $L = l_c$  ratio over smaller length scales than does the system recover the expected long length scale structure of its continuum elastic response. Based on these observations we suggest that

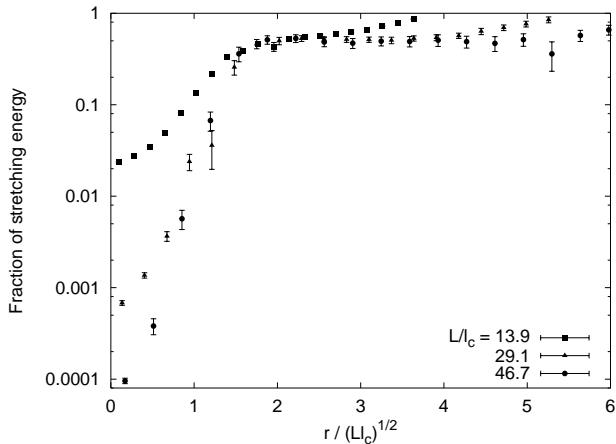


FIG .10: P roportion of elastic energy due to lam ent stretching,  $H^k = (H^k + H^2)$ , for three system s having di erent values of  $l_c$  (see key) but the same value of  $L$ .

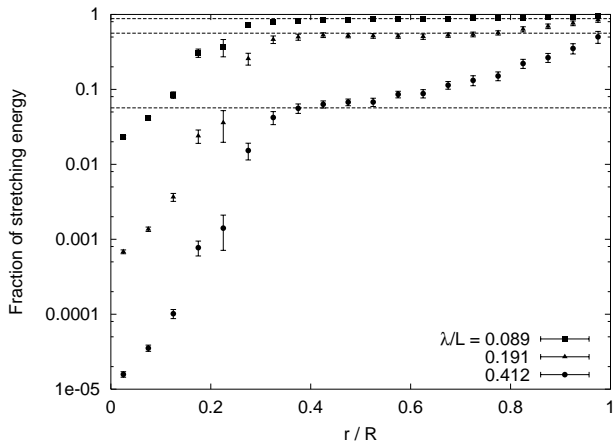


FIG .11: The fraction of elastic energy due to lam ent stretching in networks with the same  $L=l_c=29.1$  (in fact, the exact same geometries),  $R=L$  but di erent . The di erent values of the stretching energy fraction in the intermediate regime reflect the di erent values of the ratio  $L=$  for the networks. For comparison, the macroscopic energy fraction under bulk shear is shown as horizontal dashed lines, in the same order as the data points (i.e.  $=L=0.089, 0.191$  and  $0.412$  from top to bottom ).

the elastic Green's function of semi flexible gels can best be characterized as having three di erent regimes. In the immediate vicinity of the point force (near field:  $r \ll l_c$ ), the network has a complex force response (evidenced by the presence of higher angular harmonics in the Green's function) and a ratio of local bending to stretching energy density set primarily by the angle that the applied force makes with the lam ent to which that force is applied. Farther from the point force (intermediate field:  $l_c < r < L$ ) the partitioning of elastic energy reaches a value consistent with our measurements of similar systems (as defined by the value of the dimensionless ratio:

$L=$ ) under homogeneously imposed stress. Nevertheless, the structure of the response function retains higher angular harmonic terms and a dependence on the orientation of the lam ent to which the force is applied. Finally, at large distances from the point force, the structure of the displacement field appears to approach the form determined by continuum elasticity theory. Due to the size of the system explored in this work, we have better characterized the near-field and intermediate behavior of the point force response function than we have studied the far-field behavior. From basic theory, however, it is clear that this response function must approach the form given by continuum elasticity theory for isotropic media. Additionally from the intermediate regime behavior it is clear that this far-field behavior is being approached. In other words, when expanded in the angular modes as discussed above, the deformation field in the far field retains a significant amplitude in only the two modes,  $g_0^{(x)}$  and  $g_0^{(f)}$  which are predicted by continuum elasticity theory (discussed further in the appendix).

We have already shown that in the intermediate field regime the fraction of stretching elastic energy in the system approaches its far-field value as determined by the ratio:  $L=$ . Nevertheless, we in fact find that at the edges of our sample the network energy becomes stored solely in stretching modes regardless of the value of  $L=$ . As mentioned above we attribute this final redistribution of the elastic energy density between bending and stretching modes to a boundary effect imposed by the freely-rotating nature of coupling of the network lam ents to the rigid boundary. To further test that this final redistribution is indeed a boundary effect, we consider a few larger system sizes as shown in Fig. 12. In that figure the force remains perpendicular to the direction of the lam ent to which it is applied while the system size is varied from  $R=L$  to  $R=5L$  for a network of fixed  $L$ .

When the data are plotted against the radial distance from the point force scaled by system size, we find an excellent collapse in the intermediate regime and in the putative boundary layer. For the smallest system size considered,  $R=L$ , we note poorer data collapse in the near field region suggesting that one must study systems that are at least larger than a single lam ent length to access the bulk behavior of the network. Clearly, all three curves taken together are consistent with the notion of an elastic boundary layer that is produced by the freely-rotating boundary at the wall and that extends no more than a few  $l_c$  into the sample.

## 2. Far-field behavior

In order to further study the far-field behavior of the response function we turn from questions of energy partitioning to an examination of the strain field itself. In particular we compare that strain field the predictions of continuum elasticity theory. We plot  $g_0^{(f)}$  as measured from the simulations in Fig. 13 for  $=0.191L$ . It clearly

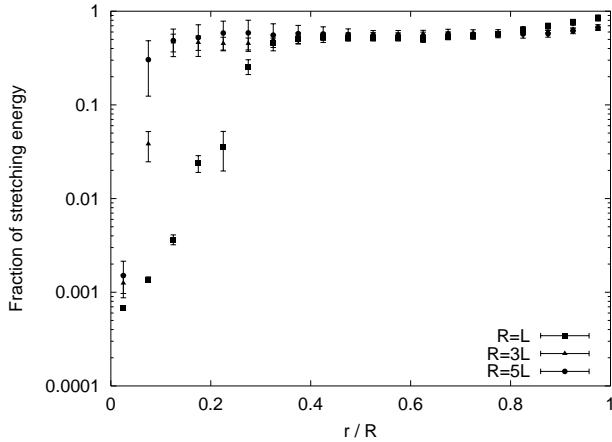


FIG. 12: The fraction of elastic energy stored in the  $H^k$  term of the Hamiltonian for perpendicular forces, as a function of distance from the origin  $r$  for system sizes  $R = L$ ,  $3L$  and  $5L$ . In all cases  $L = l_c$  29.1 and  $0.191L$ .

remain finite except at the boundary and show excellent data collapse onto a single,  $L = l_c$  independent form for three different networks (differing by  $L = l_c$ ) at the same  $r$ . In the near field, i.e. for distances  $r \ll L$  and smaller, the amplitudes of this mode depends strongly on network density  $L = l_c$ , just as for the higher angular modes discussed in Sec. II C. The data for  $g_0^{(r)}$  with  $L = 0.089L$  plotted in Fig. 14 also supports the data collapse. Although we generically find excellent data collapse for both  $g_0^{(r)}$  and  $g_0^{(f)}$  in the far field, it may be noted that there is one exceptional case as shown in Fig. 14: the data for  $L = l_c = 13.9$  does not collapse onto the universal curve as well as the other data sets that are shown. This is most likely due to the fact that  $l_c = (L = l_c) = 12.3$  so that  $l_c = 2 = 3$  and the previously assumed separation of the nonlinearity length (longitudinal correlation length) and the transverse correlation length becomes questionable. In this case we may expect that the structure of the deformation field depends on both of these lengths in a comparable manner invalidating the single-parameter scaling hypothesis underpinning the observed data collapse. This failure of the data to collapse onto a universal curve is less dramatic for all other data sets, for which  $l_c > 2.5$ . The appearance of deviations from the excellent data collapse in the case where  $l_c = 12.3$  becomes comparable further demonstrates the validity of the scaling arguments made earlier.

The collapse of  $g_0^{(r)}$  and  $g_0^{(f)}$  with  $L$  has a rather simple interpretation. Recall from the definition of the  $g^{(r)}$ 's in Eq. 3) that the shear modulus  $a$  predicted for a small deformation has already been scaled out of the data. However, as shown in our previous work [4, 7], the ratio  $a = \frac{1}{2}L$  depends only on  $L$ . Thus collapse with  $L$  in these plots is equivalent to collapse with the actual shear modulus  $a$ , just as in the solution of the continuum elasticity equations. Note that scaling by the actual  $a$  does

not collapse the data for different  $a$ , so there is additional dependency of the response function on  $a$  than just through the macroscopic elastic moduli.

We note that the monopole response approaches the same general form as the continuum solution in the intermediate regime, in the sense that the only nonvanishing angular terms in the observed deformation field correspond to terms that appear in the continuum problem. The observed amplitudes of these surviving terms, however, do not match their values determined from the continuum calculation for any system size we have been able to simulate. As an example of this discrepancy Fig. 15 shows  $g_0^{(r)}$  for a range of system sizes extending up to  $R = 7L$ . The observed amplitude is generically less (by as much as an order of magnitude) than the one calculated from the continuum elastic theory. Data for  $g_0^{(f)}$  and other system parameters obey a similar picture. Note also that the data for  $R = 3L$  and  $7L$  appears to collapse to a different curve than that of  $R = L$  used in all previous plots. A similar feature is observed for larger  $R$ . These results suggest that for large distances from the near field region of radius  $L$  about the point force the displacement field reaches a reproducible far-field value. Since we have been unable to obtain acceptable statistics in the small  $r$  range for these larger systems, we have explored this smaller ( $R = L$ ) system in detail as it remains our only way of probing the near-field response.

This apparent convergence with system size to a curve that is not predicted by the naive continuum elasticity theory can be explained as an inadequacy of the imposed boundary conditions in that calculation rather than the failure of the effective long length scale elastic theory having two Lamé coefficients. Such a theory must in fact hold as a general consequence of the isotropy of the random network. The continuum calculation assumes only that the displacement field can be derived from the minimization of an elastic energy density that depends on a gradient expansion of that displacement field having two effective Lamé coefficients. In fact our previous work and that reported here (see II C) that examines globally sheared and stretched networks indeed shows that there are two effective Lamé coefficients describing the network. The remarkable characteristic of semi-flexible networks that stands in contrast to the traditional rubber elasticity theory of flexible gels is that the Lamé coefficients of the semi-flexible network depend strongly on the length of the constituent lamellae through the dimensionless ratio:  $L = \frac{1}{2}L$ . Despite this complication involving the connection of the Lamé coefficients to the microstructure of the network, it appears prima facie that one must be able to describe the displacement field of the network at least at lengths greater than  $L$  by the continuum theory.

The remaining discrepancy between the continuum predictions and the observed displacement field as shown in Fig. 15 can be rationalized as follows. Under the localized force at the origin, the network effectively partitions itself into two different elastic materials. In the near

eld region within  $r/R$  of the point of force's application, the deformation field is not well described by any continuum elastic theory. The total force that this near field region applies to the surrounding material is equal by elementary force balance to the point force at the origin. The distribution of that total force around the boundary of the near field region is determined by local details of the network structure that certainly involves more microscopic information than is given by . In the far field where we can treat the material as some elastic continuum the problem of calculating the correct displacement field is ill-determined without details of the stresses or tractions at the inner boundary of that region with the near field region. Only by knowing such inner boundary conditions does it become possible to quantitatively predict the displacement field in the intermediate region. Nevertheless the fact that all amplitudes in this region but  $g_0^{(r)}$  and  $g_0^{(f)}$  vanish rapidly with distance from the origin shows that the material is behaving as an effective continuum material exposed to the total force  $f$ .

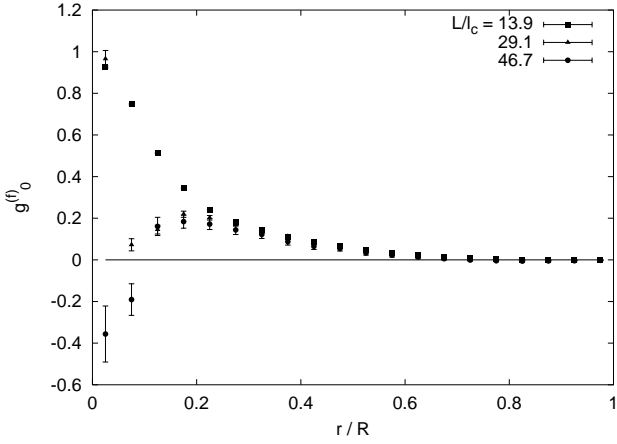


FIG. 13:  $g_0^{(f)}$  versus  $r/R$  for  $L = 0.191$ ,  $R = L$  and different  $L/l_c$ .

### B. Network response to force dipoles

We now consider the mechanical response of the network to localized force dipoles at the origin. Understanding this response function is central to elucidating the effect of molecular motor activity in the cytoskeleton. Many of the general features observed in the response of the system to point force monopoles are also in evidence. For example in Fig. 16 we see the rough collapse in the far field of the mode amplitude  $h_0^r(r)$  to the continuum solution for three different network having the same value of . Note that the amplitude has been scaled by  $l_c^2$  since the magnitude of the imposed force dipole for each realization of the network will depend on the distance to the next constraint, i.e. cross-link, which is  $l_c$ . Since the displacement field when averaged over network realiza-

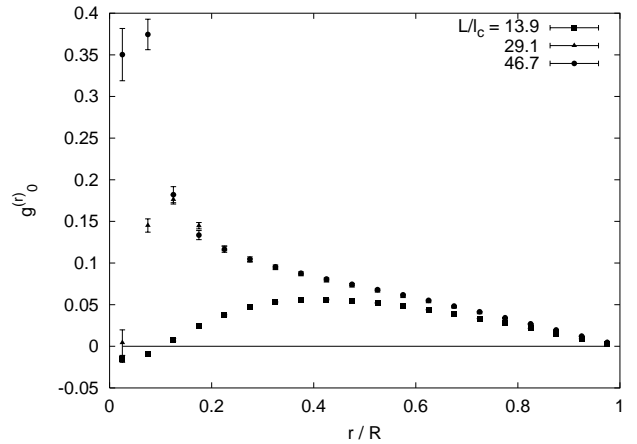


FIG. 14:  $g_0^{(r)}$  versus  $r/R$  for  $L = 0.089$ ,  $R = L$  and different  $L/l_c$ .

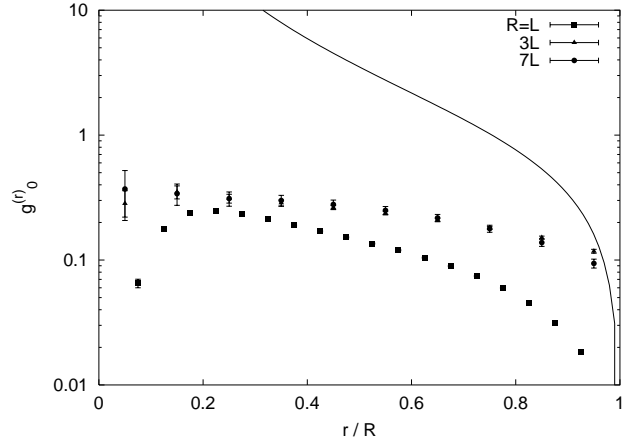


FIG. 15:  $g_0^{(r)}$  versus  $r/R$  for  $L = 0.089$ ,  $L/l_c = 29.1$  and  $R = L$ ,  $3L$  and  $7L$ . The solid line is the prediction of continuum elasticity (9).

tions is quadrupolar, being the difference in two dipole, that length must enter squared. The analogous displacement field amplitude,  $h_0^r(r)$  from the continuum solution (solid line in Fig. 16) was calculated using unit forces so this amplitude is known only up to an overall scale factor; that scale factor was adjusted to best fit the data. A similar comparison can be made for the other nonvanishing amplitudes (within the continuum approximation) of the displacement field (see the Appendix). Fig. 17, for example, shows  $h_0^f(r)$  with the same arbitrary prefactor. The agreement to the continuum theory scaled as discussed above is quite poor. More surprisingly, higher angular modes such as  $h_4^f$ , which vanish in the continuum theory, are significantly non-zero in the data.

The simulation data for the response of the network to force dipoles can be broadly summarized as follows: The amplitude of the nonvanishing angular modes of the displacement field from the naive continuum theory do not agree with simulation data. In light of the discussion

regarding such disagreements in the data on monopole data and our attribution of them to the essentially unknown boundary conditions at the boundary of the far field, this is perhaps not surprising. More interestingly, the observed displacement field has significant amplitudes of higher order angular modes. In short the universality of the response of semiregular networks to localized point forces does not appear to extend to their response to localized force dipoles.

We speculate that the principal difference between these two cases stems from the fact that the network's response to the force dipole probes the more detailed microscopic structure of the network in the immediate vicinity of the point of the force dipole application. The amplitude of the lowest order force multipole communicated from the near field region to the far field where we expect a continuum based theory to apply is not constrained by elementary force balance. Neither are the amplitudes of any higher order force multipoles generated within the near field region. Thus, upon reaching the inner edge of the far field region the force dipole imposed at the origin has generated a highly complex set of tractions on the rest of the material whose structure depends on local details of the connectivity of the network near the origin. In contrast for the case of the force monopole, the dominant term in those tractions is the fixed total monopolar force acting on the intermediate region. The higher order force multipoles created in the inner region decay rapidly with distance from the origin leaving one with highly reproducible results for the response of the network to applied forces. The amplitude of the force dipole communicated from the near field region to the intermediate region, on the other hand, is not similarly constrained. It appears that one generically generates large amplitude higher order force multipoles in addition to whatever force dipole is communicated to the intermediate region making convergence to a simple dipolar form slow and difficult to observe in our finite samples.

### C. Bulk modulus

Lastly, we present new results on homogeneous deformations of semiregular networks. It has already been shown that the macroscopic elastic modulus of this class of model networks depend in a crucial way on the ratio of  $\lambda$  to the lamellar length  $L$  [4, 7]. For  $\lambda=L=1$ , the deformation is approximately affine, whereas nonaffine deformation modes dominate when  $\lambda=L > 1$ . Previously this was demonstrated only for the shear modulus; here we can now confirm that the Young's modulus  $Y$  behaves in an identical manner. Fig. 18 shows  $Y$  measured from uniaxial extension of a rectangular cell, scaled by the prediction for an affine strain, plotted against  $\lambda=L$  for the range of  $L=l_c$  considered in this paper. There is a clear data collapse, as for the shear modulus. Furthermore the deviation from the affine prediction is small for  $\lambda=L=1$ , but becomes increasingly pronounced as  $\lambda=L$  increases.

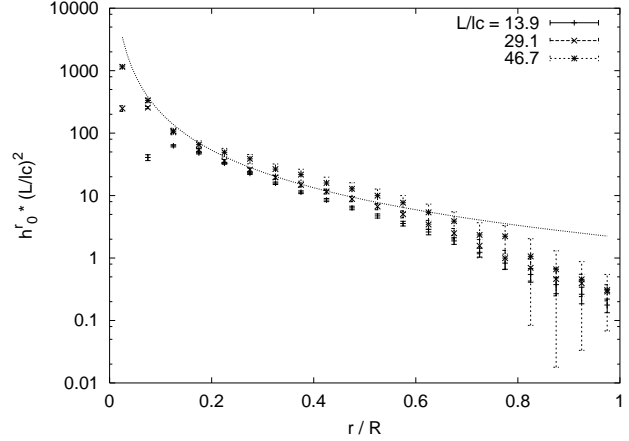


FIG. 16:  $h_0^r$  for dipole forcing for  $\lambda=L=0.191$  compared to the continuum solution (smooth line), which has one free fitting parameter, namely the overall magnitude of the dipole forcing. Both data and curve are negative, so the magnitudes have been plotted to allow use of a logarithmic axis. Each data curve has been scaled by  $(L=l_c)^2$  to ensure the same mean dipole magnitude (see text). The system radius was  $R=L$ .

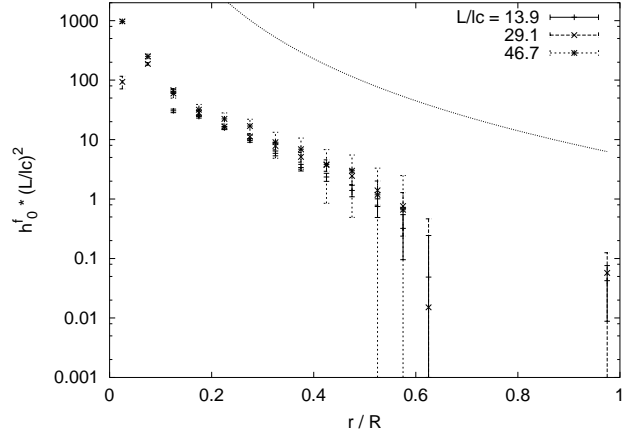


FIG. 17:  $h_0^f$  for same systems as in Fig. 16. The only fitting parameter for the continuum solution is the same as used previously for  $h_0^r$ , so there are no remaining free fitting parameters in this plot. Much of the data for  $r=R > 0.6$  is negative and hence not visible on these axes.

This confirms that  $\lambda=L$  controls the macroscopic elastic response of these systems.

Fig. 19 gives the Poisson ratio  $\nu$  for the same systems as in Fig. 18. It is striking to observe that, within error bars,  $\nu$  is consistent with the value  $\nu = \frac{1}{2}$ , which is the value expected for an affine deformation [7]. However, it is apparent from this figure that the measured values are consistent with  $\nu = \frac{1}{2}$  for all data points, even those well into the nonaffine regime. The mechanism behind this striking robustness currently evades us (it has nothing to do with incompressibility, which fixes  $\nu = 1$  in two dimensions). Note that  $\nu$  at the rigidity percola-

tion  $L=l_c = 5.933$  (at which the elastic moduli vanish) is  $\frac{1}{3}$  [6], which is clearly inconsistent with the data in Fig. 19 and confirms our earlier claim that the non-affine regime is distinct from the scaling regime of the transition.

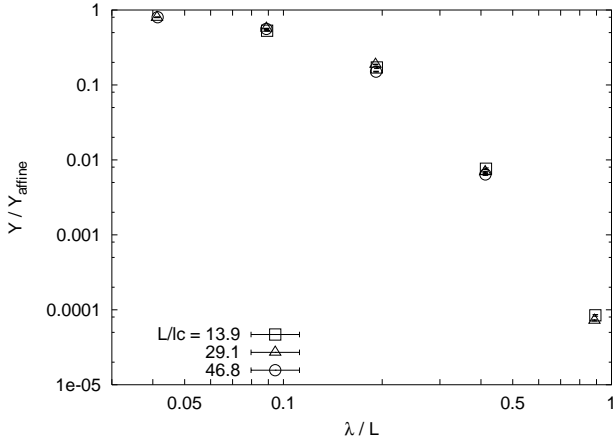


FIG. 18: Young's modulus scaled by the affine prediction versus  $\lambda/L$  on log-log axes. The affine prediction, which depends only on  $L=l_c$ , can be found in [7]. The symbols are larger than the error bars.

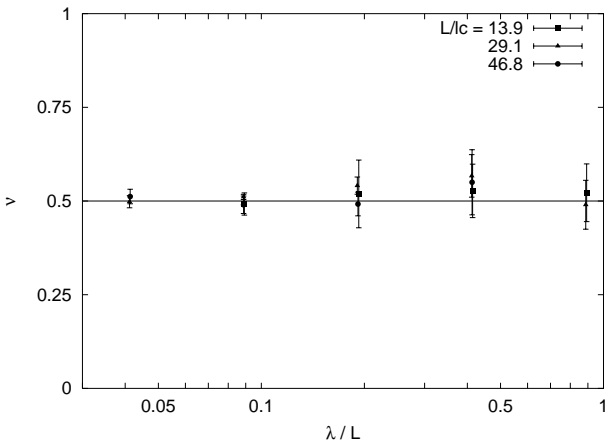


FIG. 19: The Poisson ratio  $\nu$  for the same systems as in Fig. 18. The solid line corresponds to  $\nu = \frac{1}{2}$ .

#### IV. DISCUSSION

In this paper we have presented the results of numerical studies on the response of semi-flexible networks to both point forces and to homogeneously imposed strain. The data presented on the Young's modulus taken in combination with previous work on the static shear modulus shows that the mechanical response of the system can be understood in terms of Lamé coefficients that depend on the ratio of the lamellar length to the non-affine length:

$L=l_c$ . The Poisson ratio of the material, however, appears to be remarkably insensitive to this ratio. We can offer no explanation for this insensitivity at this time. The data presented on the point force response form a necessary complement to previous work on the development of a long length scale elastic theory of such materials.

Based on these data, it appears that the storage of elastic energy and the structure of the strain field is rather complex in the immediate vicinity of the applied point force. We characterize these quantities by considering three qualitatively different regimes as a function of radial distance from the applied point force. Immediately surrounding the point force in the near-field regime we find that the partitioning of elastic energy into bending and stretching is determined primarily by the angle between the applied force and the direction of the lamellae to which that force is applied. The disorder-averaged strain field is rather complex having higher angular harmonics that predicted by continuum elasticity theory. In the intermediate field regime farther from the point force the partitioning of elastic energy is determined solely by the ratio  $L=l_c$  as found in the homogeneous shear measurements. The higher angular harmonics present in the strain field appear to decay exponentially with a decay length  $\lambda$ . These results taken in combination with our previous work suggests that one may think of  $\lambda$  as setting the minimum length scale for the applicability of continuum modelling quite generally.

In the far field we find a strain field consistent with structure of that predicted by continuum model. The strain itself, however, cannot be simply computed from a knowledge of the effective Lamé coefficients. We believe the source of this discrepancy is the fact that the intermediate region, being poorly described by the continuum theory, applies a much more complex set of tractions to the material in the far field where the continuum theory must apply. If these boundary conditions were known, we suspect that one could in fact calculate the resulting displacement field using the continuum theory. This belief is supported by the fact that in the far-field regime the displacement field for different networks having the same collapse onto the same curve as one would expect for any effective continuum theory in which the Lamé coefficients depend on  $\lambda$ .

To summarize these results, we suggest that there is an emerging description of the mechanics of semi-flexible networks. Their mechanical behavior over length scales longer than  $\lambda$  appears to be described by a modified elastic theory in which the effective Lamé constants depend on the ratio  $L=l_c$ . For point forces and presumably any force applied over regions having a characteristic length scale that is small compared to  $\lambda$ , the local response of the network is quite complex and the material appears to be anomalously compliant; at longer length scales, however, the structure of the deformation field appears to be consistent with the predictions of continuum elasticity. We believe that it should be possible to construct an elastic continuum theory of these networks that is appli-

cable in both the intermediate and far-field and that is based on a modified gradient expansion of the strain field incorporating explicitly the mesoscopic length  $\lambda$ . The behavior of the strain field on scales much smaller than  $\lambda$  appears to depend on other, more microscopic length scales.

Understanding the response of semi-exible networks to localized forces is a necessary for both microrheological investigations of semi-exible networks and for understanding the effect of molecular motors in the cytoskeleton. Clearly, further numerical investigations are required as well as a theoretical examination of the development of elastic continuum models applicable to the intermediate and far-field regimes.

Moreover, additional investigations are required to examine the analogous questions in three dimensional semi-exible networks. While we expect the basic physics outlined above, including the existence of a mesoscopic length  $\lambda$ , to persist in three dimensions, the expected  $1/r$  decay of the elastic Green's function should alter the results. Moreover the more rapid decay of the displacement field and energy density in the continuum three dimensional system may further simplify the structure of the analogous Green's functions for the semi-exible network.

#### Acknowledgments

A JL and FCM acknowledge the hospitality of the Isaac Newton Institute for Mathematical Sciences where part of this work was done. D AH was jointly funded by the European Community Marie Curie and the Japanese Society for the Promotion of Science programs. A JL was supported in part by nsf-dm r0354113.

#### APPENDIX

Here we derive the displacement field  $u(x)$  predicted by continuum elasticity for the cases of both monopole and dipole forcing. For the monopole case, a point force  $f(x)$  is applied to the origin of an elastic sheet with Lamé coefficients and  $\nu$ , or equivalently  $\lambda$  and the Poisson ratio  $\nu = (2 + \lambda)/3$ . For an isotropic elastic body, the stress obeys  $\sigma_{ij} = (\lambda u_j + \nu u_i) + \delta_{ij} r^{-1} u$  and the resulting equation for force balance is [18]

$$(\lambda + \nu) \delta_{ij} (r^{-1} u) + r^2 u_{ij} = f_i(x); \quad (7)$$

Solving this in polar coordinates  $(r, \theta)$  with the boundary condition  $u = 0$  at a radius  $R$  from the origin eventually leads to

$$u_i^{\text{mono}} = \frac{f}{8} r^2 \left[ 4\hat{f}_i \ln(r/R) + 4q \hat{f}_i \hat{f}_j \hat{f}_j + c_2(r/R)^2 \left( 2\hat{f}_i \hat{f}_j \hat{f}_j - \frac{1}{r} \right) \right] + \frac{1}{8} \left( \frac{f}{r} \right)^2 \left( 2\hat{f}_i \hat{f}_j \hat{f}_j - \frac{1}{r} \right); \quad (8)$$

where  $c_1 = (1 + \nu)/(3 - \nu)$  and  $q = (5 + \nu)/(3 - \nu)$ . Then the only two non-zero modes according to the definition of the  $g^{(r)}$  given in (4) are

$$g_0^{(r)} = \frac{a}{8} r^2 \left[ 4q + 2c_2(r/R)^2 - 2(r/R)^2 \right]; \quad (9)$$

$$g_0^{(F)} = \frac{a}{8} r^2 \left[ 4 \ln(r/R) - q(r/R)^2 + c_2(r/R)^2 \right]; \quad (10)$$

A naive calculation of the corresponding dipole solution would simply superpose the above monopole solution for two point forces,  $f(x)$  and  $f(x')$  with  $x' = \hat{f}$ , and then take the limit  $x' \rightarrow 0$ . However, this ignores the boundary at radius  $R$ , which should be kept fixed but is shifted a distance  $\lambda$  by the above procedure. An exact calculation would require the monopole solution for force applied near to (but not at) the center of a circular system, which, since it no longer obeys radial symmetry, is likely to be highly complex. Here we ignore such issues and simply use the above monopole solution, in the expectation that it will closely approximate the exact case except possibly near the boundary. The displacement field induced by the force dipole is then

$$\begin{aligned} u_i^{\text{dip}} &= \frac{1}{\pi} r u_i^{\text{mono}} \\ &= \frac{f}{8} \frac{1}{r} \left[ \hat{f}_i (4c_1 - 2q(r/R)^2 + 2(r/R)^2) \right. \\ &\quad + 8\hat{f}_i (\hat{f} \cdot \hat{f})^2 c_2(r/R)^2 q \\ &\quad \left. + 2\hat{f}_i (\hat{f} \cdot \hat{f}) (2(c_1 - 1) - 2q(r/R)^2) \right. \\ &\quad \left. (q - 1)(r/R)^2 \right]; \quad (11) \end{aligned}$$

As explained in Sec. II C, the dipole solution above applies for a single realization on large length scales, but after averaging over many networks on short lengths (as in the simulations) the dipole moment vanishes, leaving a quadrupole displacement field. The required quadrupole is one consisting of two parallel dipoles of equal and opposite magnitude, aligned along their axes, i.e.

$$\begin{aligned} u_i^{\text{quad}} &= \frac{1}{\pi} r u_i^{\text{dip}} \\ &= \frac{f}{8} \frac{1}{r^2} \left[ \hat{f}_i (4(2c_1 - 1) - 6q(r/R)^2) \right. \\ &\quad + 2(2 - q)(r/R)^2 \\ &\quad + 24\hat{f}_i (\hat{f} \cdot \hat{f}) c_2(r/R)^2 q \\ &\quad + 8\hat{f}_i (\hat{f} \cdot \hat{f})^2 (1 - 2q + 3c_2(r/R)^2) \\ &\quad \left. + 16\hat{f}_i (\hat{f} \cdot \hat{f})^3 (2c_1 - 3q(r/R)^2) \right]; \quad (12) \end{aligned}$$

This gives the displacement field in response to known forces of magnitude  $f$ . Since it is rather the displacement that is controlled,  $f$  is a free parameter. Finally, the non-

zero modes are

$$h_0^{(r)} = \frac{a_{ne}}{r^2} \frac{1}{r} \overset{\circ}{q} ; \quad (13)$$

$$h_2^{(r)} = \frac{a_{ne}}{2} \frac{1}{r^2} 2c_1 - 3\overset{\circ}{q} (r=R)^2 ; \quad (14)$$

$$h_0^{(f)} = \frac{a_{ne}}{4} \frac{1}{r^2} 3c_2 (r=R)^2 + (2 - \overset{\circ}{q}) (r=R)^2 ; \quad (15)$$

$$h_2^{(f)} = \frac{a_{ne}}{4} \frac{1}{r^2} 1 - 2\overset{\circ}{q} + 3c_2 (r=R)^2 : \quad (16)$$

[1] B. A. Alberts, D. Bray, J. Lewis, M. Ra, K. Roberts, and J.D. Watson, *Molecular Biology of the Cell*, 3rd edition (Garland, New York, 1994); P.A. Janmey *Curr. Opin. Cell Biol.* 3, 4 (1991).

[2] E.L. Elson *Annu. Rev. Biophys. Biochem.* 17, 397 (1988).

[3] M. Rubenstein and R.H. Colby, *Polymers Physics* (Oxford University Press, London, 2003).

[4] D.A. Head, A.J. Levine and F.C. MacKintosh, *Phys. Rev. Lett.* 91, 108102 (2003).

[5] J. Wilhelm and E. Frey, *Phys. Rev. Lett.* 91, 108103 (2003).

[6] D.A. Head, F.C. MacKintosh and A.J. Levine, *Phys. Rev. E* 68, 025101(R) (2003).

[7] D.A. Head, F.C. MacKintosh and A.J. Levine, *Phys. Rev. E* 68, 061907 (2003).

[8] Alex J. Levine, D.A. Head, and F.C. MacKintosh *J. Phys.: Condens. Matter.* 16, S2079 (2004).

[9] K. Kroy and E. Frey, *Phys. Rev. Lett.* 77, 306 (1996).

[10] F.C. MacKintosh, J. Kas and P.A. Janmey, *Phys. Rev. Lett.* 75, 4425 (1995).

[11] J.P. Wittmer, A. Tanguy, J.-L. Barrat and L. Lewis, *Europhys. Lett.* 57, 423 (2002).

[12] A. Tanguy, J.P. Wittmer, F. Leonforte and J.-L. Barrat, *Phys. Rev. B* 66, 174205 (2002).

[13] F. Leonforte, A. Tanguy, J.P. Wittmer and J.-L. Barrat, *Phys. Rev. B* 70, 014203 (2004).

[14] C. Bustamante, J.F. Marko, E.D. Siggia, and S. Smith, *Science* 265, 1599 (1994).

[15] W.H. Press, S.A. Teukolsky, W.T. Vetterling and B.P. Flannery, *Numerical recipies in C*, 2nd ed. (CUP, Cambridge, 1992).

[16] P.R. Onck, T. Koeman, T. van Dillen and E. van der Giessen, cond-mat/0502397.

[17] D. Bray, *Cell Movements: From molecules to motility*, 2nd ed. (Garland, New York, 2001).

[18] L.D. Landau and E.M. Lifshitz, *Theory of elasticity*, 3rd ed. (Reed, Oxford, 1986).